BBA - Biomembranes 1863 (2021) 183570

Contents lists available at ScienceDirect

BBA - Biomembranes

journal homepage: www.elsevier.com/locate/bbamem

Insertion state of modular protein nanopores into a membrane

Motahareh Ghahari Larimi [a], Jeung-Hoi Ha [b], Stewart N. Loh [b], Liviu Movileanu [a,c,*]

[a] Department of Physics, Syracuse University, 201 Physics Building, Syracuse, NY 13244-1130, USA
[b] Department of Biochemistry and Molecular Biology, State University of New York - Upstate Medical University, 4249 Weiskotten Hall, 766 Irving Avenue, Syracuse, NY 13210, USA
[c] Department of Biomedical and Chemical Engineering, Syracuse University, 329 Link Hall, Syracuse, NY 13244, USA

ARTICLE INFO

Keywords:
FhuA
Protein engineering
Single-molecule electrophysiology
Protein dynamics
Outer membrane protein
Monomer
Membrane protein reconstitution

ABSTRACT

In the past decade, significant progress has been made in the development of new protein nanopores. Despite these advancements, there is a pressing need for the creation of nanopores equipped with relatively large functional groups for the sampling of biomolecular events on their extramembranous side. Here, we designed, produced, and analyzed protein nanopores encompassing a robust truncation of a monomeric β-barrel membrane protein. An exogenous stably folded protein was anchored within the aqueous phase via a flexible peptide tether of varying length. We have extensively examined the pore-forming properties of these modular protein nanopores using protein engineering and single-molecule electrophysiology. This study revealed distinctions in the nanopore conductance and current fluctuations that arose from tethering the exogenous protein to either the N terminus or the C terminus. Remarkably, these nanopores insert into a planar lipid membrane with one specific conductance among a set of three substate conductance values. Moreover, we demonstrate that the occurrence probabilities of these insertion substates depend on the length of the peptide tether, the orientation of the exogenous protein with respect to the nanopore opening, and the molecular mass of tethered protein. In addition, the three conductance values remain unaltered by major changes in the composition of modular nanopores. The outcomes of this work serve as a platform for further developments in areas of protein engineering of transmembrane pores and biosensor technology.

1. Introduction

In the last two decades, nanopore sensing has emerged as a powerful technology for single-molecule detection, as well as for DNA and RNA sequencing. This method uses the ability to measure a tiny electrical current and its discrete fluctuations through a single biological nanopore or a synthetic nanopore [1,2]. Despite significant progress on utilizing nanopores for studying unfolded polymers, such as poly(ethylene glycol) (PEG), polysaccharides, DNA, RNA, unfolded proteins, and polypeptides, there is modest advancement on the development of nanopore sensors capable of sensing large globular proteins interacting with other proteins in solution. This is mainly because most folded proteins have a radius larger than the nanopore internal diameter [3–5]. For example, the most widely used biological nanopore (αHL) has an average internal diameter of ~2 nm and constriction size of ~1.4 nm [6]. Larger protein nanopores, such as α-helical cytolysin A (ClyA) [7,8] and two-component pleurotolysin AB (PlyAB) [9], have been also employed for investigating globular proteins and their interactions with other reactive partners. ClyA features an extended diameter of approximately ~5.5 nm, whereas PlyAB has *trans* and *cis* openings of ~7 nm and ~ 10 nm, respectively. Yet, confining a large protein inside a nanopore to study its interaction with other protein analytes may decrease the accessibility of the binding domain and increase the low-entropy confinement, impairing the kinetics of the native interactions. Moreover, the protein must reside inside the nanopore for a satisfactorily long time to be able to interact with its partner.

To overcome this barrier, the concept of sensing outside the nanopore has attracted increased attention. This approach usually requires a chemical or a genetic modification of the nanopore. Bayley and coworkers (2000) attached a PEGylated biotin to the interior of an αHL vestibule using chemical modification via a reactive cysteine sulfhydryl. In this case, a biotin on the untethered PEG end captured a high-affinity streptavidin and other anti-biotin antibodies with various binding affinities [10]. The same research group has extended this elegant

* Corresponding author at: Department of Physics, Syracuse University, 201 Physics Building, Syracuse, NY 13244-1130, USA.
E-mail address: lmovilea@syr.edu (L. Movileanu).
URL: http://movileanulab.syr.edu (L. Movileanu).

https://doi.org/10.1016/j.bbamem.2021.183570
Received 21 November 2020; Received in revised form 6 January 2021; Accepted 13 January 2021
Available online 30 January 2021

detection mechanism of single proteins outside the pore lumen [11] via attached aptamers [12] and fused reactive peptides [13,14]. As a follow-up work to these studies, Chen and coworkers (2015) attached the PEGylated biotin to the rim of an outer membrane protein G (OmpG) nanopore [15,16] and showed that the sensitivity and selectivity of this sensor for protein detection could be tuned by altering the length of the PEG tether [17]. This successful work was also an extension from multimeric nanopores to a monomeric nanopore [18,19]. However, the common aspect of these nanopore designs is the relatively small size of the tethered ligand, such as an organic molecule [10,15,17], a DNA aptamer [12], or a short peptide [13,14]. Recently, Thakur and Movileanu (2019) [20] showed that barnase-barstar interactions [21–27] could be sampled outside the nanopore via a genetically encoded monomeric protein nanopore sensor. In this design, a barnase protein, which is a small 110-residue RNase, was genetically engineered to the N terminus of a truncated derivative of ferric hydroximate uptake component A (t-FhuA) [28] via a Gly-Ser hexapeptide tether. Attachment of a small polypeptide tail on the N terminus of barnase modulated the characteristic electrical signature of the barnase-t-FhuA nanopore. Binding of barstar, an 89-residue protein inhibitor, to the barnase domain of the barnase-t-FhuA nanopore further changed the electrical signature [20,29], facilitating a quantitative determination of the kinetics of barnase-barstar interactions at single-molecule precision.

Yet, the design of a nanopore with an external tethered protein for sampling different protein-protein pairs remains a challenging task due to a number of physicochemical reasons of the engineered recognition protein domain. These include its size and charge distribution, as well as the location of the binding interface of both proteins with respect to the tethering terminus of the nanopore. In addition to these complicated design issues, it is not clear whether the overall construct can form a stable pore-forming protein, whose functional properties can be modified in a desired direction and in a tractable fashion. Therefore, it is imperative to better understand how the conductance properties of a globular protein domain-containing protein nanopore change when its composition is altered in a systematic manner.

In this work, we extended these prior redesign studies [20] by developing a number of modular nanopores that encompassed t-FhuA (Fig. 1AB) [20,28]. The wild-type protein, FhuA, is a 22-stranded, monomeric, β-barrel outer membrane protein in *E. coli* [30,31]. Our earlier studies have revealed that FhuA derivatives insert into a planar lipid membrane in a single orientation [20,28,32,33]. For example, if we consider the *cis* and *trans* sides of the chamber and the FhuA derivative was added to the *cis* side, then the short β-turns faced the *cis* side, whereas the long extracellular loops were located on the *trans* side. Cellular rapidly accelerated fibrosarcoma-RAS binding domain (CRAF1-RBD), a 76-residue ubiquitin-like protein [34–36], was chosen as an exogenous folded protein domain owing to its high thermodynamic stability [34] (Fig. 1C). Hence, CRAF1-RBD is a stably folded protein under physiological conditions. In contrast to our previously published study on the single-molecule detection of protein-protein interactions [20], CRAF1-RBD was fused on the extramembranous side of t-FhuA via a flexible Gly-Ser-rich peptide linker of varying length. This protein served as an external movable plug of the nanopore (Fig. 1AB). Thus, we created a modular nanostructure encompassing a redesigned transmembrane β-barrel scaffold and a water-soluble exogenous folded protein. Because of the asymmetric charge distribution of CRAF1-RBD with respect to the longitudinal axis of the N to C terminus (Fig. 1C), we were able to explore the outcomes of protein fusion to either terminus of t-FhuA. The N and C termini of t-FhuA are both accessible to the *cis* side of the protein and they are within a distance of ~8 Å apart from each other.

Here, we provide experimental evidence for differences in the single-channel electrical signature of nanopores when the fusion was conducted to either the N or C terminus. We tested these modular protein nanopores using 3-, 6-, and 9-residue peptide tethers for fusing CRAF1-RBD to t-FhuA (Fig. 1, Table 1). An immediate outcome of this work is that the varying length of the peptide tether and the orientation of the movable plug with respect to the nanopore opening have a significant effect on the nanopore's characteristic electrical signature. This can be in the form of either improving or impairing the electrical quietness of the open-state current of inspected nanopores. Finally, a slightly negatively charged polypeptide tail was fused at the untethered terminus of the CRAF1-RBD-containing nanopore. In this way, we show that different tethered molecular mass might affect the most probable insertion substate of modular nanopores.

2. Materials and methods

2.1. Cloning, expression, and purification of t-FhuA-based nanopores

The *HRAS* binding domain of CRAF1, also named CRAF1-RBD, was fused to t-FhuA via a Gly/Ser-rich hexapeptide tether ($(GGS)_2$). CRAF1-RBD was amplified from pQE32 RAF-DHFR [37,38] (kindly provided by S.W. Michnik) using the following PCR primer pair: 5′-CTTTA AGAAG GAGAT ATACA AATGA GCAAC ACTAT CCGTG TTTTC-3′ (forward) and 5′-GGCTG CCGCC GCTGC CGCCG AAATC TACTT GAAGT TCTTC TCC-3′ (reverse).

The PCR product was purified on agarose gel and inserted at the N terminus of $(GGS)_2$-t-FhuA in pPR-IBA1 by a Restriction Free cloning procedure [39]. All the sequence was verified by DNA sequencing (Supporting Information, Supporting Methods). R9F, F9R and F9R14 were synthesized by Genscript (Piscataway, NJ). F6R27 and F3R24 were synthesized by ABclonal (Woburn, MA). The gene sequences were further confirmed by the DNA sequencing service of GenScript Biotech (Piscataway, NJ). All genes were subcloned in the pPR-IBA1 expression vector (IBA, Goettingen, Germany). They were transformed into *E. coli* BL21(DE3) (New England Biolabs, Ipswich, MA) for protein expression. Transformed cells were grown in LB medium at 37 °C until OD_{600} reached a value of ~0.4.

Protein expression was induced by 0.5 mM isopropyl *β*-D-1-thio-galctopyranoside (IPTG) (Gold Biotechnology®, Inc., St Louis, MO) at 37 °C. After induction, cells were grown for an additional period of 4–5 h at 37 °C, just until the cell growth reached the plateau saturation. Then, cells were harvested by centrifugation at 3700 ×*g* for 30 min at 4 °C. This centrifugation step was followed by cell resuspension in 10 ml of 500 mM KCl, 5 mM EDTA, 50 mM Tris, pH 8, 20 mM β-mercaptoethanol (βME) per each gram of cells. Cell lysis was conducted using a model 110 L microfluidizer (Microfluidics, Newton, MA) for ~20 times. Cell lysates were centrifuged at 25,000 ×*g* for 45 min at 4 °C to separate the pellet from supernatant. Since all synthetic protein nanopores were expressed as inclusion bodies, the pellets were further washed with 300 mM KCl, 5 mM EDTA, 50 mM Tris-HCl, 20 mM βME, pH 8.0. This was followed by one wash in 300 mM KCl, 5 mM EDTA, 50 mM Tris-HCl, 20 mM βME, 1% (*v*/v) Triton-X, pH 8.0, two washes in 1 M urea, 50 mM Tris-HCl, 20 mM βME, pH 8.0, one wash in 2 M urea, 50 mM Tris-HCl, 20 mM βME, pH 8.0, and two final washes in 50 mM Tris-HCl, 5 mM TCEP, pH 8.0. Resuspended pellet was homogenized by a Dounce homogenizer at 4 °C for 30 min, then centrifuged at 25,000 ×*g* for 45 min at 4 °C. The final pellet was solubilized in 8 M urea, 50 mM Tris-HCl, 5 mM TCEP, pH 8.0, for at least 12 h before its loading on an anion-exchange column. Solubilized pellet was spun down at 25,000 ×*g* for 30 min at 20 °C, then passed through a 0.2 μm filter (Corning, Glendale, AZ) to remove insoluble impurities.

Protein sample was loaded on an anion-exchange column, Model Bio-scale MT20 (Bio-Rad, Hercules, CA), which was packed with UNO-sphere Q Resin (Bio-Rad), and equilibrated with 8 M urea, 50 mM Tris-HCl, 5 mM TCEP, pH 8.0. Protein was eluted by 200 ml of KCl gradient from 0 to 500 mM. All the protein samples were eluted around 120–140 mM KCl. Fractions were run on the SDS-PAGE for protein detection and purity analysis. Fractions containing the pure sample were pooled out and dialyzed against ddH_2O (MilliporeSigma, Burlington, MA). Dialyzed samples were lyophilized using a model Freezone 2.5 L Labcono freeze dryer (Labcono, Kansas City, MO) for long time storage at −20 °C.

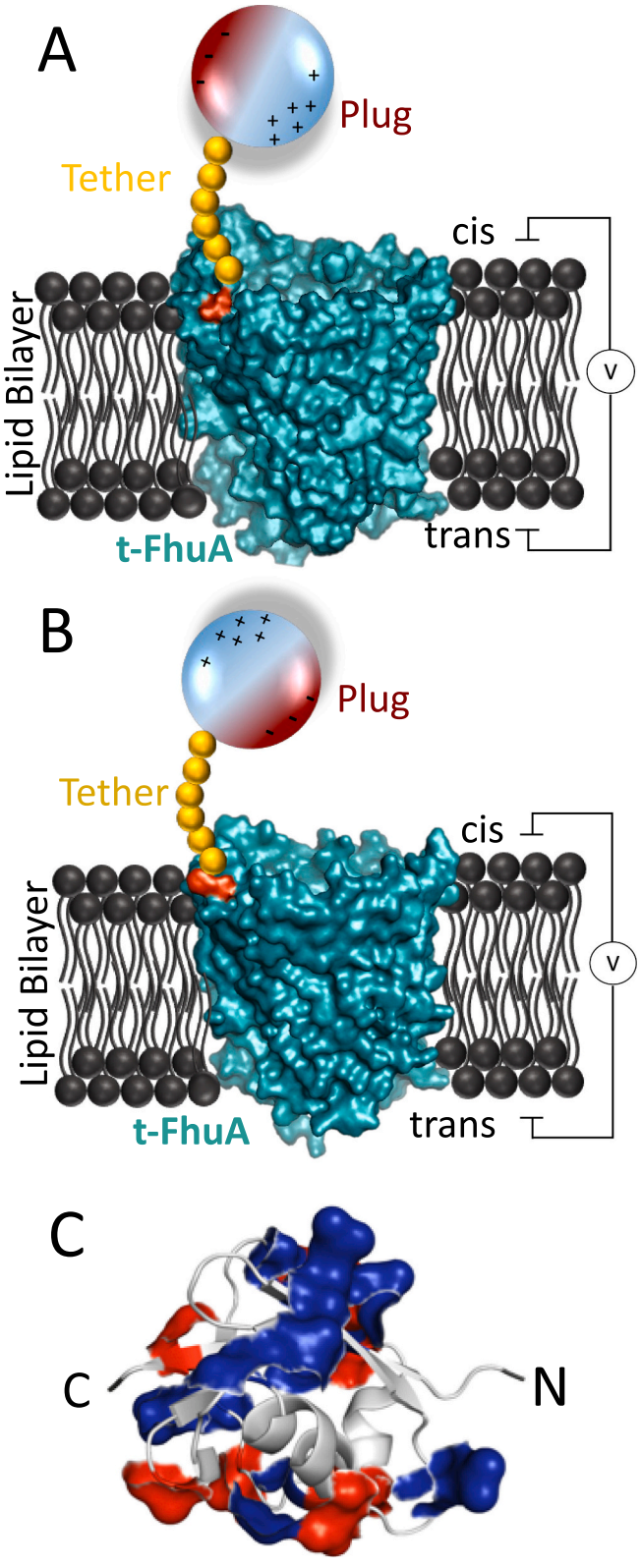

(caption on next column)

Fig. 1. Schematic of CRAF1-RBD-containing modular nanopores reconstituted in a planar lipid membrane. An asymmetrically charged folded CRAF1-RBD domain [36,43,44] (external plug) was fused to either the N terminus (A) or to the C terminus (B) of t-FhuA [20,28] via a flexible Gly/Ser-rich peptide tether of varying length. Fusion of the folded CRAF1-RBD domain to either the N terminus or to the C terminus reorients the location of different charges of the external plug with respect to the *cis* opening of t-FhuA. In (A) and (B), the locations of the N and C terminus of t-FhuA (marked in cyan) are indicated in red, respectively. (C) The structure of the folded CRAF1-RBD domain (pdb code: 4g0n) [49] that illustrates the asymmetric charge distribution with respect to the N to C terminus axis. In (C), positively charged residues and negatively charged residues are shown in blue and red, respectively. (For interpretation of the references to colour in this figure legend, the reader is referred to the web version of this article.)

2.2. Preparation of CRAF1-RBD

Tether and t-FhuA were deleted from R6F plasmid by PCR using a Q5 site-directed mutagenesis kit (New England Biolabs) with forward primer 5′-TAAAGCGCTTGGAGCCACCCGCAGTTCGAA-3′ and reverse primer 5′-GAAATCTACTTGAAGTTCTTCTCCAATCAAAGACGC-3′. Sequences were further confirmed by the DNA sequencing service of Genscript Biotech. CRAF1-RBD in pPR-IBA1 vector was transformed into *E. coli* BL21(DE3) cells. Transformed cells were grown in LB medium at 37 °C until OD_{600} reached a value of ~0.4. Temperature was brought down to 20 °C for 30 min. Protein expression was induced by 0.5 mM of IPTG (Gold Biotechnology®) at 20 °C for at least 16 h. Then, cells were centrifuged at 3700 ×*g* for 30 min at 4 °C. Pellet was resuspended in 10 ml of 300 mM KCl, 50 mM Tris-HCl, 20 mM βME, pH 8.0 per each gram of cells. Cell lysis was conducted using a Model 110 L Microfluidizer (Microfluidics, Newton, MA) for 20 times. Cell lysates were centrifuged at 25,000 ×*g* for 45 min at4°C to separate the pellet from supernatant. Supernatant was furthered processed using 10% (*w/v*) of ammonium sulfate precipitation at 4 °C, which was followed by 40% (w/v) of ammonium sulfate precipitation. Protein sample was dialyzed against 50 mM Tris-HCl, 1 mM TCEP, pH 7.0 for running on an ion-exchange chromatography column (UNOsphere Q, Bio-Rad, Hercules, CA). Proteins samples were eluted by a linear gradient of 0 to 500 mM KCl. Protein samples were concentrated using a 3 kDa-cut off concentrator (Pierce protein concentrator-PES, Thermo Fisher Scientific, Waltham, MA). Proteins were purified using size-exclusion chromatography on a HiLoad 16/600 Superdex 75 pg column (GE Healthcare, Chicago, IL) in 50 mM Tris-HCl, 1 mM TCEP, pH 8.0. Protein fractions were further concentrated and stored at −80 °C.

2.3. Preparation of Q61L-HRAS

HRAS plasmid subcloned in a PET41b vector was obtained from GenScript Biotech. Single-point mutation on residue Q61L-HRAS was made using a Q5 site-directed mutagenesis kit (New England Biolabs) as well as the following PCR primers: 5′-ACAGCTGGTCTAGAAGAATATTCT −3′ (forward) and 5′-ATCCAAGATATCCAACAAACAA −3′ (reverse). The mutant sequence was confirmed by the DNA sequencing service of GenScript Biotech. Expression of Q61L-HRAS and cell lysis were conducted in a manner closely similar to that used for CRAF1-RBD, except that the lysis buffer included 10 mM $MgCl_2$. After the centrifugation of cell lysates, the supernatant was run on a polyhistidine-tag affinity column, Model Bio-Scale Mini Profinity IMAC Cartridge (Bio-Rad). Then, the eluted protein was run through size-exclusion chromatography using a HiLoad 16/600 Superdex 75 pg column (GE Healthcare, Chicago, IL) for further purification and buffer replacement. Protein sample, which was resuspended in 100 mM KCl, 30 mM Tris-HCl, 10 mM $MgCl_2$, pH 8, was concentrated for its reaction with a non-hydrolysable GTP reagent, GppNHp (Abcam, Cambridge, UK). Final protein sample was dialyzed against ddH_2O and lyophilized for storage at −20 °C. To load the Q61L-HRAS with GppNHp, lyophilized sample

Table 1
Physicochemical properties of various modular protein nanopores explored in this study. In all abbreviations, F stands for t-FhuA (Supporting Information, Supporting Methods) [20,28]. For the abbreviation of various modular nanopores, R represents the folded CRAF1-RBD domain fused at either the N terminus (it shows on the left side of F) or at the C terminus (it shows on the right side of F) of t-FhuA. The number located on either the left side or right side of F indicates the length of the flexible peptide tether (e.g., provided in the number of amino acids). This peptide tether was fused to either the N terminus or the C terminus of t-FhuA, respectively (Supporting Information, Supporting Methods). Some modular protein nanopores, whose folded CRAF1-RBD domain was fused at the C terminus of t-FhuA (via a peptide linker), included a C-terminal polypeptide tail. These modular single-polypeptide chain nanopores are externally functionalized, because the hydrophilic CRAF1-RBD protein is expectedly located outside the nanopore interior. This approach contrasts to traditionally conducted internal functionalization of nanopores [48].

Synthetic protein nanopore	t-FhuA terminus for protein fusion	Number of residues in the tether	The stretched length of the tether (Å)	Number of residues in the tail	The stretched length of the tail (Å)	Total number of added residues[b]	Net tethered charge
R6F	N	6	21	N/A	N/A	82	2.8
R9F	N	9	31.5	N/A	N/A	85	2.8
F9R	C	9	31.5	N/A	N/A	85	2.8
F9R14[a]	C	9	31.5	14	49	99	0.8
F6R27[a]	C	6	21	27	94.5	109	−2.2
F3R24[a]	C	3	10.5	24	84	103	−1.2

[a] This number on the right side of R stands for the number of residues present in the C-terminal polypeptide tail (Supporting Information, Supporting Methods).
[b] These numbers represent the total numbers of residues added to t-FhuA in each construct.

was resuspended in buffer containing 50 mM KCl, 30 mM Tris-HCl, 1 mM EDTA, pH 8.0. 50 U calf intestinal alkaline phosphatases were added per 10 mg of proteins. Subsequently, GppNHp was added at a concentration 10-fold higher than the protein concentration. The sample was incubated at 37 °C for 1 h. To stabilize the binding of GppNHp to protein, 20 mM of $MgCl_2$ was added to the sample. Afterward, buffer was exchanged with 50 mM KCl, 20 mM Mg Cl_2, 20 mM Tris-HCl, 5 mM DTT, pH 8.0. Protein samples were quantified using a reducing agent-compatible Pierce® Microplate BCA Protein Assay Kit (Thermo Fisher Scientific, Waltham, MA).

2.4. Refolding of protein nanopores

Lyophilized samples were solubilized in 8 M urea, 200 mM KCl, 50 mM Tris-HCl, 5 mM TCEP, pH 8.0 for at least 4 h at room temperature. Samples were quantified by the UV absorbance at a wavelength of 280 nm using a microplate reader, Model SpectraMax I3 (Molecular Devices, LLC., San Jose, CA). 1.5% (*w/v*) n-dodecyl-β-D-maltopyranoside (DDM) (Anatrace, Maumee, OH) was added to the denatured protein samples at a concentration in the range of 20–30 μM. Protein samples were then refolded through a slow-dialysis process against 200 mM KCl, 50 mM Tris-HCl, 1 mM TCEP, pH 8.0 over a 5-day duration.

2.5. Single-channel electrical recordings with planar lipid bilayers

Single-channel electrical recordings were performed, as previously described [40,41]. The *cis* and *trans* compartments were separated by a 25 μm-thick Teflon film (Goodfellow Corporation, Malvern, PA), which contained a 100 μm-diameter orifice. This aperture was treated with 10% (*v/v*) hexadecane (Sigma-Aldrich, St. Louis, MO) dissolved in pentane (Sigma-Aldrich). 10 μl of 10 mg/ml 1,2-diphytanoyl-*sn*-glycerophosphocholine (Avanti Polar Lipids, Alabaster, AL) was added to form a planar lipid bilayer across the aperture. The *cis* and *trans* compartments were filled with 1.5 ml of 300 mM KCl, 10 mM $MgCl_2$, 10 mM Tris, pH 8, 0.5 mM TCEP (or DTT), unless otherwise stated. Protein sample was added to the *cis* chamber up to the final concentration of 1–2 ng/μl. The *cis* compartment was grounded. Electric pulses of 220–260 mV were applied for durations of shorter than 10 s to facilitate protein insertion. Single-channel electrical traces were acquired using a patch-clamp amplifier, Model Axopatch 200B (Axon Instruments, Foster City, CA) in the whole-cell mode ($\beta = 1$) using a CV-203BU headstage. Single-channel electrical traces were digitized by Digidata 1440 A/D convertor (Axon Instruments). The signal was low-pass filtered using an 8-pole Bessel filter (Model 900, Frequency Devices, Haverhill, MA) at a frequency of 10 kHz and sampled at a rate of 50 kHz. Single-channel electrical traces were later analyzed using pClamp 10.7 (Axon Instruments) and Origin v9.65 (2019b) (OriginLab Corporation, Northampton, MA). All measurements were performed at room temperature (23 ± 0.5 °C).

3. Results

3.1. t-FhuA, the β-barrel stem of modular protein nanopores

In this results section, we show data in the form of unitary conductance measured through single protein nanopores [1,2]. In addition, the method of single-channel electrical recordings (the Materials and Methods section) enabled us to probe discrete current fluctuations of individually-inspected modular nanopores. In general, the single-channel conductance of our synthetic nanopores followed a three-peak distribution. The signature of this three-peak conductance distribution strongly depended on the nature of modular architecture of each nanopore. Under these conditions, the nanopore stem, t-FhuA (Table 1; Supporting Information, Supporting Methods) [20,28], showed one minor low-conductance peak and two major large-conductance peaks (Fig. 2A). Peak 1, Peak 2, and Peak 3 of t-FhuA exhibited average conductance values of 0.4 ± 0.1 nS ($n = 9$), 0.9 ± 0.1 nS ($n = 29$), 1.5 ± 0.1 nS ($n = 22$), respectively, making their relative frequencies of the insertion substate of ~15%, ~48%, and ~ 37%, respectively (Table 2, Fig. 2A). The unitary conductance and relative frequency of the insertion substate of t-FhuA nanopores, which corresponded to individual peaks, was provided in Table 2. At a transmembrane potential of +40 mV, the low-conductance Peak 1 was populated by short-lived and frequent current blockades with a dwell time, an event frequency, and a normalized amplitude of 0.8 ± 0.2 ms, 141 ± 12 s^{-1}, and ~ 0.7, respectively ($n = 3$). Here, the normalized current amplitude is defined by $\Delta I/I_0 = (I_0 - I)/I_0$, where I_0 and I are the single-channel electrical currents recorded for the open substate and partly-closed substate of Peak 1, respectively. This intrinsic gating of t-FhuA was symmetric with respect to the voltage bias. For example, Peak 1 was featured by closely similar events with a dwell time of 0.9 ± 0.2 ms, an event frequency of 135 ± 26 s^{-1}, and a normalized amplitude of ~0.6 at a transmembrane potential of −40 mV (n = 3) (Supporting Information, Table S1, Fig. S1A—B). On the other hand, the medium-conductance Peak 2 exhibited short-lived and time-unresolvable current spikes (Fig. 2B, Supporting Information, Fig. S1C). Remarkably, Peak 3 was characterized by a quiet and stable single-channel electrical signature for long periods (Fig. 2C; Supporting Information, Fig. S1D).

3.2. Tethering CRAF1-RBD to the N terminus of t-FhuA

First, we examined a synthetic nanopore containing a CRAF1-RBD domain fused to the N terminus of t-FhuA via a medium-sized Gly/Ser-rich hexapeptide tether, also named R6F (Table 1). Remarkably, the

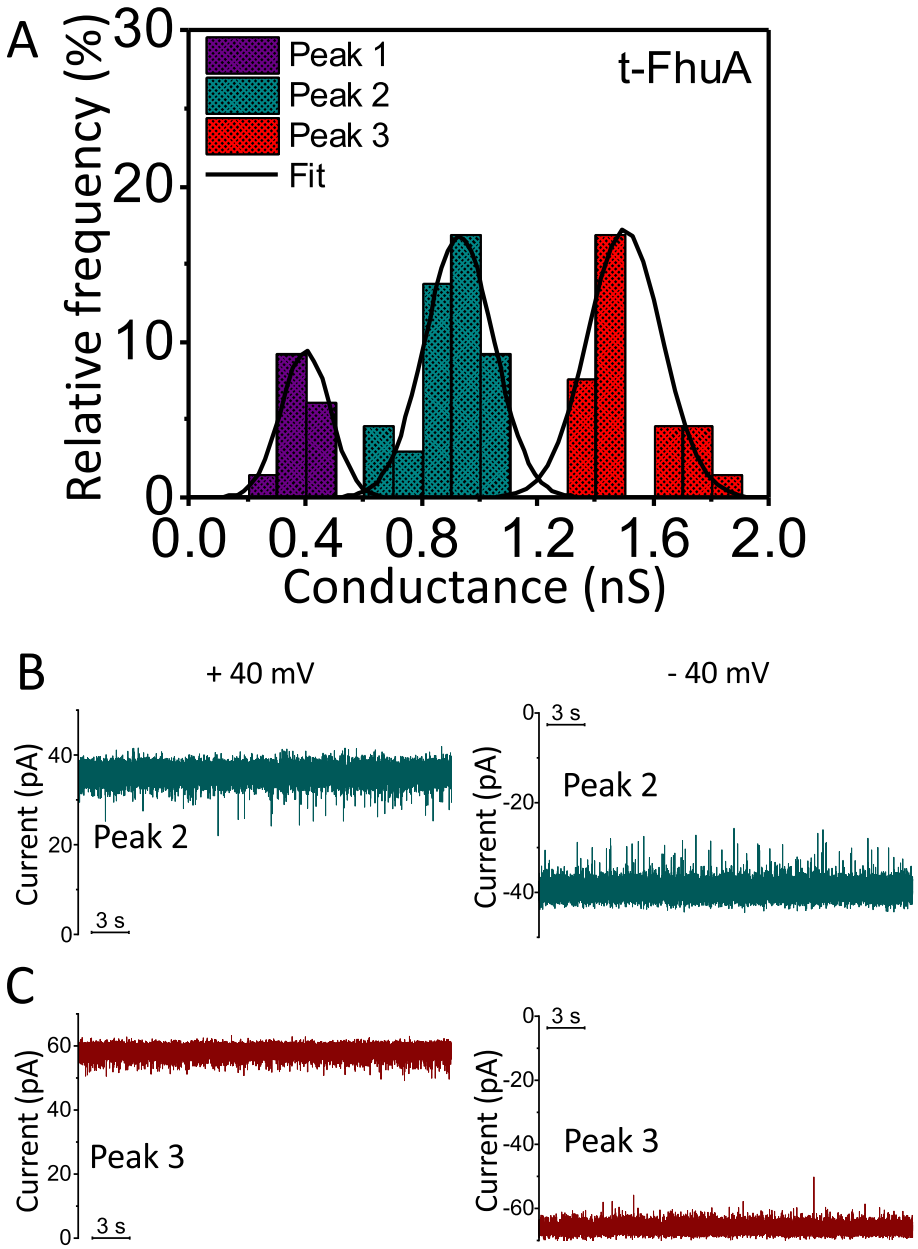

Fig. 2. Single-channel electrical recording of t-FhuA. (A) Histogram of the single-channel conductance values of various peak clusters recorded with t-FhuA. Clusters of the low-conductance Peak 1, medium-conductance Peak 2, and large-conductance Peak 3 of t-FhuA were centered at ~0.4 nS (purple), ~0.9 nS (cyan), and ~ 1.5 nS (red), respectively. The applied transmembrane potential was +40 mV. (B) Representative single-channel electrical traces of the medium-conductance Peak 2 cluster of t-FhuA at a transmembrane potential of +40 mV (*left*) and − 40 mV (*right*). (C) Representative single-channel electrical traces of the large-conductance Peak 3 cluster of t-FhuA at a transmembrane potential of +40 mV (*left*) and − 40 mV (*right*). These electrical traces were low-pass filtered at 3 kHz using an 8-pole Bessel filter. (For interpretation of the references to colour in this figure legend, the reader is referred to the web version of this article.)

distribution of individual peak clusters and their specific signature was altered with respect to those of the unmodified t-FhuA nanopore (Table 2, Fig. 3A). As a control experiment, it was tested whether the quiet signature of t-FhuA from the Peak 3 cluster was affected by the presence of the tethering CRAF1-RBD, here also called the plug (Fig. 1AB). Specifically, t-FhuA nanopore from the Peak 3 cluster did not show any transient or permanent closure upon the addition of 10 μM CRAF1-RBD to the *cis* side at applied transmembrane potentials of +40 mV and – 40 mV (Supporting Information, Fig. S2). Peak 1, Peak 2, and Peak 3 of R6F exhibited average conductance values of 0.4 ± 0.1 nS (n = 8), 0.9 ± 0.1 nS (n = 16), 1.3 ± 0.1 nS (n = 11), respectively, making their relative frequencies of the insertion substate of ~23%, ~46%, and ~ 31%, respectively (Table 2, Fig. 3A). The low-conductance Peak 1 and medium-conductance Peak 2 showed signatures closely similar to those of t-FhuA (Supporting Information, Table S1, Fig. S3A—C). R6F nanopores of the large-conductance Peak 3 cluster inserted into the bilayer as a single-step process, as noted by a discrete increase in the single-channel electrical current (Supporting Information, Fig. S3D). This means that R6F nanopores of Peak 3 are not immediately related to R6F nanopores of Peak 1 and Peak 2 in terms of their pore-forming properties. Furthermore, R6F nanopores of the large-conductance Peak 3 displayed current blockades with a relative current amplitude of 0.24 ± 0.02, a dwell time of 0.10 ± 0.03 ms, and an event frequency of 18 ± 14 s^{-1} at a transmembrane potential +40 mV (n = 4) (Supporting Information, Fig. S4). These single-channel parameters were 0.22 ± 0.01, 0.10 ± 0.06 ms, and 11 ± 5 s^{-1}, respectively, at a potential of −40 mV (n = 3). Because t-FhuA nanopores of the large-conductance Peak 3 cluster showed a quiet single-channel electrical signature, contrasting to R6F nanopores, it is likely that CRAF1-RBD interacts with the opening of R6F nanopores, creating reversible single-channel current blockades.

Next, we explored a CRAF1-RBD-containing modular nanopore that featured a 9-residue Gly/Ser-rich peptide linker (R9F, Table 1). The stretched-out conformation of this linker measures ~31 Å assuming a distance of ~3.5 Å in between individual side chains. Peak 1, Peak 2, and Peak 3 of R9F exhibited average conductance values of 0.4 ± 0.1 nS (n = 9), 0.9 ± 0.1 nS (n = 21), and 1.5 ± 0.2 nS (n = 8), respectively,

Table 2
Distribution of various peak clusters of the different modular protein nanopores examined in this work. Displayed conductance substates were determined at a transmembrane potential of +40 mV. The low-conductance Peak 1 cluster spanned a single-channel conductance range of 0–0.6 nS. The medium-conductance Peak 2 cluster ranged between 0.6 and 1.0 nS. The large-conductance Peak 3 cluster covered a single-channel conductance range of 1.0–1.6 nS. The first line indicates the average single-channel conductance of the peak cluster, *G*, which was provided as mean ± s.d. The second line indicates the relative frequency, *P*, of the insertion substate, which is followed by the number of independently acquired data points from distinct experiments.

Synthetic protein nanopore		Peak 1 *G* (nS) *P* (%; n)	Peak 2 *G* (nS) *P* (%; n)	Peak 3 *G* (nS) *P* (%; n)	Most probable peak
t-FhuA		0.4 ± 0.1 (15%; n = 9)	0.9 ± 0.1 (48%; *n* = 29)	1.5 ± 0.1 (37%; *n* = 22)	Peak 2
N terminus	R6F	0.4 ± 0.1 (23%; *n* = 8)	0.9 ± 0.1 (46%; *n* = 16)	1.3 ± 0.1 (31%; *n* = 11)	Peak 2
	R9F	0.4 ± 0.1 (24%; *n* = 9)	0.9 ± 0.1 (55%; *n* = 21)	1.5 ± 0.2 (21%; *n* = 8)	Peak 2
C terminus	F9R	0.4 ± 0.1 (42%; *n* = 17)	0.8 ± 0.1 (35%; *n* = 14)	1.5 ± 0.2 (23%; n = 9)	Peak 1
	F9R14	0.4 ± 0.1 (15%; *n* = 5)	0.8 ± 0.1 (24%; n = 8)	1.4 ± 0.1 (64%; n = 21)	Peak 3
	F6R27	N/A[a]	0.8 ± 0.1 (25%; n = 8)	1.4 ± 0.1 (75%; *n* = 24)	Peak 3
	F3R24	0.4 ± 0.1 (21%; n = 9)	0.9 ± 0.1 (33%; n = 14)	1.5 ± 0.1 (46%; *n* = 19)	Peak 3

[a] N/A stands for Not Applicable.

making their relative frequencies of ~24%, ~55%, and ~ 21%, respectively (Table 2, Fig. 4A). Again, signatures of R9F nanopores of the low-conductance Peak 1 and medium-conductance Peak 2 were closely similar to those of t-FhuA (Supporting Information, Table S1, Fig. S5A—C). The large-conductance R9F nanopores inserted into lipid bilayer within a single-step process, as revealed by a well-defined, discrete current change (Supporting Information, Fig. S5D). Yet, these R9F nanopores showed a noisy signature at a potential of −40 mV (Fig. 4C; Supporting Information, Fig. S6).

3.3. Tethering CRAF1-RBD to the C terminus of t-FhuA

Then, we investigated nanopores that featured the fusion of CRAF1-RBD to the C terminus of t-FhuA. First, we employed a 9-residue Gly/Ser-rich flexible peptide tether, as in the above-described example. These nanopores were called F9R (Table 1). In this case, the low-conductance Peak 1 become the most probable cluster with a relative insertion frequency of ~42% (Table 2, Fig. 5A). The characteristics of the nanopores belonging to Peaks 1 and 2 were closely similar to other nanopores presented above (Table S1, Supporting Information, Fig. S7A—C). F9R nanopores of the large-conductance Peak 3 cluster exhibited a relative insertion frequency of ~23% and an average single-channel electrical conductance of 1.5 ± 0.2 nS (n = 9). Interestingly, these large-conductance F9R nanopores exhibited a quiet and stable single-channel electrical signature for long periods (Fig. 5D; Supporting Information, Fig. S7D, Fig. S8).

Next, we engineered a 14-residue polypeptide tail at the C terminus of CRAF1-RBD, resulting in a newly redesigned nanopore, also called F9R14 (Table 1). This design strategy enabled us to unravel whether additional molecular mass of the tethered protein domain has any effect on the most probable conductance value of the insertion substate. This C-terminal tail is an unstructured and slightly negatively charged polypeptide (Supporting Information, Supporting Methods) [42]. In this case, a total of 99 residues are tethered at the C terminus. Surprisingly, the presence of a 14-residue unstructured tail on the F9R nanopore produced a significant alteration in the cluster distribution. Peak 1, Peak 2, and Peak 3 were centered at average conductance values closely similar to those of the other modular nanopores (Table 2). Yet, F9R14 nanopores of the large-conductance Peak 3 became the most probable with a relative frequency of ~64% (Fig. 5B). The low-conductance Peak 1 and medium-conductance Peak 2 only showed relative frequencies of 15% and 24%, respectively. F9R14 nanopores of the Peak 1 cluster exhibited signatures almost identical to the other modular nanopores (Supporting Information, Table S1, Fig. S9A—B).

Remarkably, those F9R14 nanopores of the Peak 2 and Peak 3 clusters revealed quiet and stable single-channel electrical signatures for long periods (Supporting Information, Fig. S9C, Fig. S10). These quiet electrical signatures of the F9R14 nanopores indicated that the 14-residue tail does not create a noisier electrical signature, a phenomenon previously encountered with the barnase-t-FhuA nanopore under a similar experimental condition (the Introduction section) [20]. Therefore, we hypothesized that the polypeptide tail was not reaching the nanopore opening or it was pointed away from the nanopore opening. In addition, we tested whether potential interactions between the 14-residue polypeptide tail and the charges of the nanopore opening are detectable at a lower salt of concentration of 150 mM KCl. Under this condition, we noted a single-peak cluster of F9R14 nanopores whose single-channel conductance was ~0.8 nS (n = 16) (Supporting Information, Fig. S11). This unitary conductance value corresponds to that of the Peak 3 cluster acquired in a buffer solution containing 300 mM KCl (Table 2). Moreover, F9R14 nanopores showed a quiet and stable single-channel electrical signature for long periods. Even if a noisier signal exists at a very low salt concentration, a likely reduced signal-to-noise ratio under these conditions would prevent its discrimination from other noise sources of the system.

In light of the results acquired with F9R and F9R14 nanopores, we decided to employ a shorter 6-residue Gly/Ser-rich flexible tether, which restrained the moieties of CRAF1-RBD nearer the pore opening. In addition, we engineered a 27-residue length tail at the C terminus of the pore, also called F6R27 (Table 1; Supporting Information, Supporting Methods). Surprisingly, F6R27 showed only two major peak clusters. Peak 2 exhibited an average conductance of 0.8 ± 0.1 nS (n = 8) and a relative insertion frequency of ~17% (Table 2, Fig. 5C). The large-conductance Peak 3, with a relative insertion frequency of ~75%, was centered at 1.4 ± 0.1 nS (n = 24). Again, the single-channel electrical signature of Peak 3 resembled the signature of other modular nanopores with quiet signatures (Supporting Information, Fig. S12–S13), indicating that the 27-residue polypeptide tail was also pointed away from the pore opening. Q61L-HRAS is an oncogenic mutant of the small GTPase HRAS that exhibits a binding interaction with its protein effector CRAF1-RBD [36,43,44]. We found that the addition of 400 nM Q61L-HRAS to the *cis* side of the chamber created short-lived and frequent current blockades at an applied transmembrane potential of −40 mV (Supporting Information, Fig. S14A). The addition of Q61-HRAS to the *cis* compartment did not produce any change in the quiet signatures of the Peak 3 clusters of F9R14 (Supporting Information, Fig. S14B) and t-FhuA (Supporting

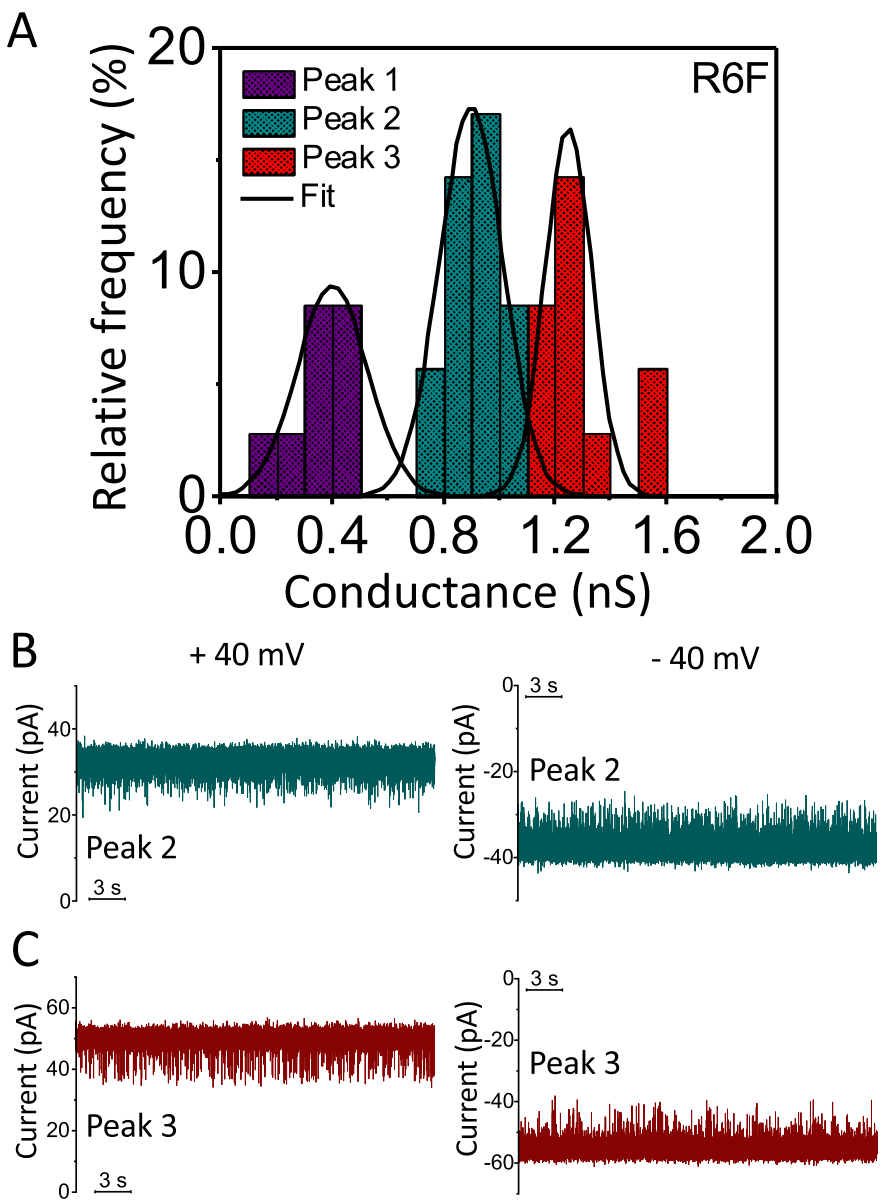

Fig. 3. Single-channel electrical recording of R6F. (A) Histogram of the single-channel conductance values of various peak clusters recorded with R6F. Clusters of the low-conductance Peak 1, medium-conductance Peak 2, and large-conductance Peak 3 of R6F were centered at ~0.4 nS (purple), ~0.9 nS (cyan), and ~ 1.3 nS (red), respectively. The applied transmembrane potential was +40 mV.
(B) Representative single-channel electrical traces of the medium-conductance Peak 2 cluster of R6F at a transmembrane potential of +40 mV (*left*) and − 40 mV (*right*). (C) Representative single-channel electrical traces of the large-conductance Peak 3 cluster of R6F at a transmembrane potential of +40 mV (*left*) and − 40 mV (*right*). These electrical traces were low-pass filtered at 3 kHz using an 8-pole Bessel filter. (For interpretation of the references to colour in this figure legend, the reader is referred to the web version of this article.)

Information, Fig. S14C).

Finally, we inquired how a further reduction in the tether length affects the distribution and electrical signature of nanopores of different peak clusters. Specifically, we redesigned a modular protein nanopore with a short 3-residue peptide tether at the C terminus of t-FhuA and a long 24-residue polypeptide tail at the untethered end of CRAF1-RBD (Supporting Information, Supporting Methods), also called F3R24. Thus, we observed again a three-peak distribution of the F3R24 nanopores with single-channel conductance values closely similar to those of t-FhuA (Table 2, Fig. 5D). Finally, in this case nanopores of the Peak 3 cluster were the most probable, with a relative insertion frequency of ~46%. Furthermore, Peak 1 and Peak 2 showed signatures that were almost similar to the other modular nanopores (Supporting Information, Fig. S15A-C). Signatures of nanopores of the Peak 3 cluster were also quiet for long periods (Supporting Information, Fig. S15D, Fig. S16).

4. Discussion

In this paper, we systematically explored a new class of modular protein nanopores with an exogenous folded protein located within the extramembranous side. These methodical manipulations outside the pore lumen included alterations in the length of the peptide tether, changes in the orientation of the folded protein with respect to the pore opening, and modifications in the molecular mass of the tethered protein. The untethered β-barrel nanopore, t-FhuA, as well as the other six CRAF1-RBD-containing protein nanopores exhibited one of the three insertion substates when reconstituted into a planar lipid membrane. These were a low-conductance substate (e.g., a low-conductance nanopore), a medium-conductance substate (e.g., a medium-conductance nanopore), and a large-conductance substate (e.g., a large-conductance nanopore). For each modular nanopore configuration, the conductance substate was a fixed value, so that the occurrence probability was the insertion probability in each conductance substate. In other words, once inserted into the membrane, a single nanopore does not fluctuate among the three conductance substates. Therefore, the reported relative insertion frequencies in Table 2 do not reflect any transition between two conductance substates. Single-channel conductance values of these nanopores were centered around ~0.4 nS (Peak 1), ~0.9 nS (Peak 2), and ~ 1.5 nS (Peak 3), respectively. Yet, the sum of relative insertion frequencies of protein nanopores with a medium-

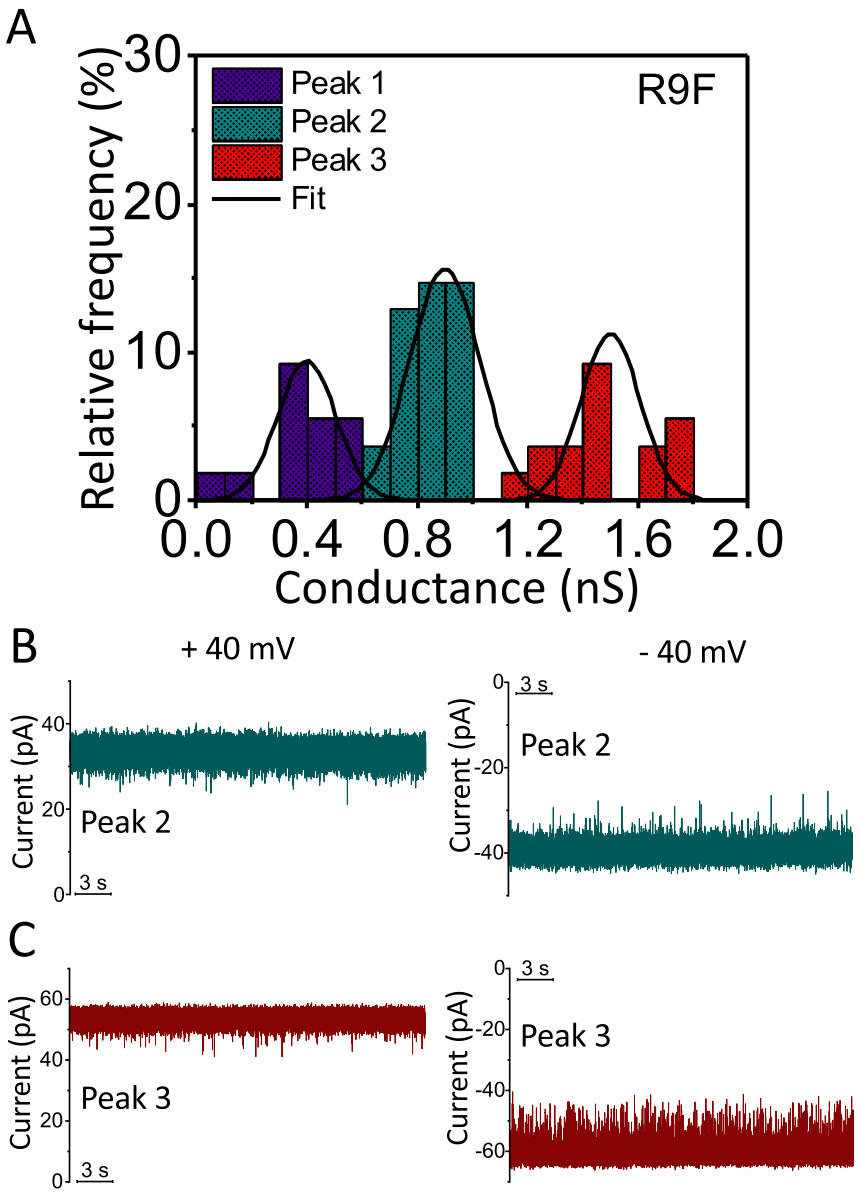

Fig. 4. Single-channel electrical recording of R9F. (A) Histogram of the single-channel conductance values of various peak clusters recorded with R9F. Clusters of the low-conductance Peak 1, medium-conductance Peak 2, and large-conductance Peak 3 of R9F were centered at ~0.4 nS (purple), ~0.9 nS (cyan), and ~ 1.5 nS (red), respectively. The applied transmembrane potential was +40 mV.
(B) Representative single-channel electrical traces of the medium-conductance Peak 2 cluster of R9F at a transmembrane potential of +40 mV (*left*) and − 40 mV (*right*).
(C) Representative single-channel electrical traces of the large-conductance Peak 3 cluster of R9F at a transmembrane potential of +40 mV (*left*) and − 40 mV (*right*). These electrical traces were low-pass filtered at 3 kHz using an 8-pole Bessel filter. (For interpretation of the references to colour in this figure legend, the reader is referred to the web version of this article.)

conductance substate (Peak 2) and a large-conductance (Peak 3) ranged between 58% (F9R) and 100% (F6R27). This finding indicates that these two substates together are the most probable for all examined nanopores.

Interestingly, the t-FhuA terminus at which the CRAF1-RBD protein was fused was a major determinant for the characteristics of these modular nanopores. Thus, nanopores with features of Peak 2 were observed with highest relative insertion frequency when the protein fusion was conducted at the N terminus of t-FhuA. On the contrary, nanopores with features of Peak 3 were noted with highest relative insertion frequency in three out of the four cases when the protein fusion was executed at the C terminus. These clearly distinct outcomes concerning the fusion terminus were acquired regardless of the tethered molecular mass and regardless of the length of peptide tether. We think that there are two possible tentative interpretations of these results. First, the movements of the tethered protein at the tip of modular nanopore generate an external repulsion force on the t-FhuA terminus, such as that performed by an elastic entropic string [45]. For example, this force is an exclusion force from the pore lumen, which also exists in the absence of the tethering. Yet, this strain is transmitted across the peptide tether in the presence of the tethering. This physical interaction can generate an entropic force up to several pN [46]. It is conceivable that the resulting strain on the N terminus affects the overall structure of t-FhuA with respect to the situation when the resulting strain acts on the C terminus. Second, the moieties of CRAF1-RBD at the tip of the nanopore might also be impacted by local electrostatic interactions with the charges located on the short β turns of the nanopore opening. Therefore, a second mechanism of the alterations of the nanopore insertion state might be determined by distinctions in electrostatic distribution of CRAF1-RBD with respect to the t-FhuA terminus at which it is fused.

Indeed, we noted that there is a charge asymmetry with respect to the N to C terminus axis (Fig. 1). This asymmetric charge distribution might also affect the local interactions in the proteomicelle containing the protein nanopore and detergent molecules, in this case n-dodecyl-β-D-maltopyranoside (DDM). The 76-residue long CRAF1-RBD, sequence 55–130, includes localized clusters of positively charged residues (R58, R67,R73, H79,R89, R99, H102,H104, R111) and negatively charged residues (D80, E94,E102, D113, D117, E124, E125, D129). In Fig. 6A, we show how the positively charged residues of CRAF1-RBD potentially face the acidic side chains on the β turns of the nanopore stem when the

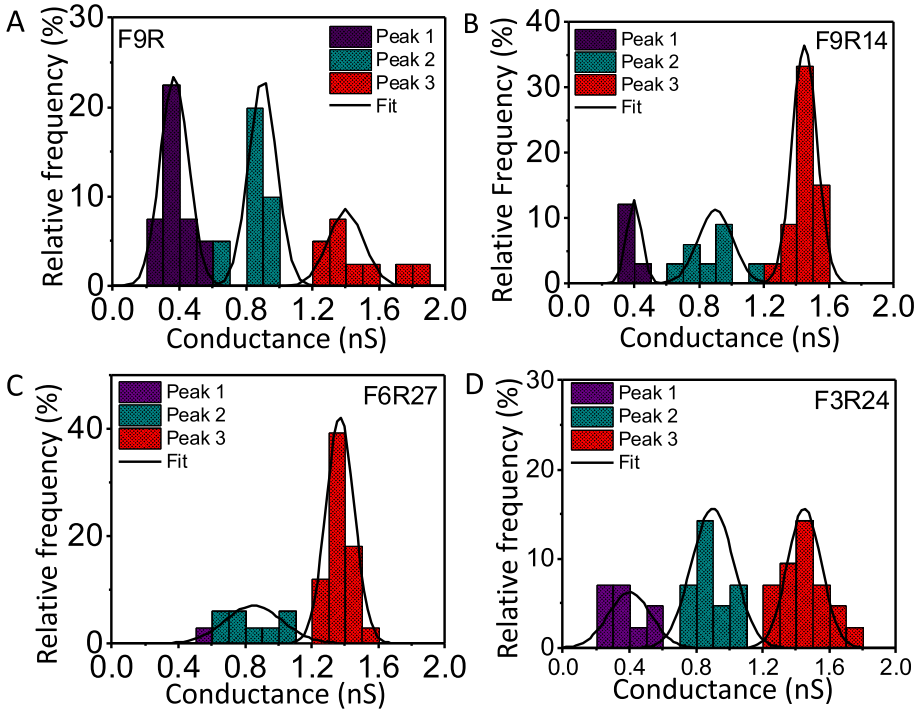

Fig. 5. Single-channel conductance histograms of CRAF1-RBD-containing modular nanopores show an amplification in the relative insertion probability when protein fusion was conducted at the C terminus. (A) Histogram of the single-channel conductance values of various peak clusters recorded with F9R. Clusters of the low-conductance Peak 1, medium-conductance Peak 2, and large-conductance Peak 3 of F9R were centered at ~0.4 nS (purple), ~0.8 nS (cyan), and ~1.5 nS (red), respectively. (B) Histogram of the single-channel conductance values of various peak clusters recorded with F9R14. Clusters of the low-conductance Peak 1, medium-conductance Peak 2, and large-conductance Peak 3 of F9R14 were centered at ~0.4 nS (purple), ~0.8 nS (cyan), and ~1.4 nS (red), respectively. (C) Histogram of the single-channel conductance values of various peak clusters recorded with F6R27. Clusters of the medium-conductance Peak 2 and large-conductance Peak 3 of F6R27 were centered at ~0.8 nS (cyan), and ~1.4 nS (red), respectively. (D) Histogram of the single-channel conductance values of various peak clusters recorded with F3R24. Clusters of the low-conductance Peak 1, medium-conductance Peak 2, and large-conductance Peak 3 of F3R24 were centered at ~0.4 nS (purple), ~0.9 nS (cyan), and ~1.5 nS (red), respectively. The applied transmembrane potential was +40 mV. (For interpretation of the references to colour in this figure legend, the reader is referred to the web version of this article.)

protein fusion was conducted at the N terminus of t-FhuA. On the other hand, if the C terminus was employed for protein fusion, then such potential electrostatic interactions between the external surface of CRAF1-RBD and the nanopore entrance would be much less likely. In support to this second postulated mechanism, the nanopores R6F and R9F that belonged to the large-conductance Peak 3 cluster, when the fusion at the N terminus of t-FhuA was conducted, showed a very noisy electrical signature (Figs. 3 and 4). Yet, this result contrasted with that obtained with nanopores that belonged to the large-conductance Peak 3 cluster of t-FhuA (Fig. 2).

Furthermore, the fusion of CRAF1-RBD at the C terminus not only increased the relative insertion frequencies of substates corresponding to the large-conductance Peak 3 cluster, but also produced a quieting of the large-conductance substate (Supporting Information, Fig. S8, Fig. S10, Fig. S12, Fig. S16). Again, this finding was in contrast to the outcomes of single-molecule electrophysiology experiments when the fusion was conducted at the N terminus of t-FhuA. The fact that the large-conductance state is quiet in all four C terminus-fused nanopores, F9R, F9R14, F6R27, and F3R24, regardless of the tether length and regardless of tethered molecular mass, is consistent with the lack of significant attraction interactions at the CRAF1-RBD - t-FhuA interface. In contrast, such potential interactions were observed in the form short-lived current blockades for the two N terminus-fused nanopores (Figs. 3 and 4). This finding is in accordance with an increased relative insertion frequency of large-conductance nanopores and a decreased relative insertion frequency of medium-conductance nanopores when the fusion was conducted at the C terminus of t-FhuA. However, we found that the most probable low-conductance Peak 1 cluster of F9R nanopores is surprising, in light of these findings and our tentative-tone interpretations. Nevertheless, the large-conductance R9F and F9R nanopores that belonged to Peak 3 occurred with a closely similar relative insertion frequency.

In this study, we have also examined whether a change in the tethered molecular mass affects the relative insertion frequency of the C terminus-fused modular nanopores. Therefore, we engineered polypeptide tails at the untethered terminus of CRAF1-RBD. Remarkably, the relative insertion frequency of large-conductance nanopores was drastically amplified from 23% to 64% when a 14-residue unstructured polypeptide tail was engineered at the C terminus of F9R nanopore. This amplification was further extended to 75% for F6R27, a nanopore with a 6-residue peptide linker and a 27-residue polypeptide tail. Moreover, a low-conductance insertion state was not observed with a F6R27 nanopore. F3R24, a nanopore with a very short 3-residue peptide linker and a 24-residue long unstructured tail yet exhibited a most probable large-conductance Peak 3 cluster. These findings demonstrate that the lengths of the peptide tether and polypeptide tail are also key determinants for the likelihood of the insertion substate of a modular protein nanopore. Furthermore, the engineering of polypeptide tails at the C terminus of CRAF1-RBD did not produce any statistically significant change in the magnitude and electrical signature of the high-conductance insertion substate with respect to that of t-FhuA. Quiet large-conductance insertion substates of polypeptide tail-containing protein nanopores suggest that these engineered polypeptide tails do not physically reach the nanopore opening (Fig. 6B).

This new class of modular and single-polypeptide chain protein nanopores is useful for both protein engineering and design of biosensors for the detection of proteins and protein-protein interactions outside the pore lumen. However, the design of a nanopore for a specific protein-protein pair remains a challenging task due to a number of reasons, including the physicochemical features of the engineered binding protein domain, such as its size, charge distribution, and location of the binding interface of both proteins with respect to the tethering terminus. The last property becomes critical for the accessibility of tethered binding domain by the targeted protein analyte. To design a universal sensor, the parameters that potentially affect the structural and functional features of these genetically encoded protein nanopores should be known. Another essential parameter to consider is the length of the peptide tether between the recognition protein domain and nanopore. On one hand, these two domains must be far enough to have a certain degree of freedom. On the other hand, they must be in a relatively close proximity for the sensor to be functional. Therefore, determining the length of a tether that simultaneously serves these purposes

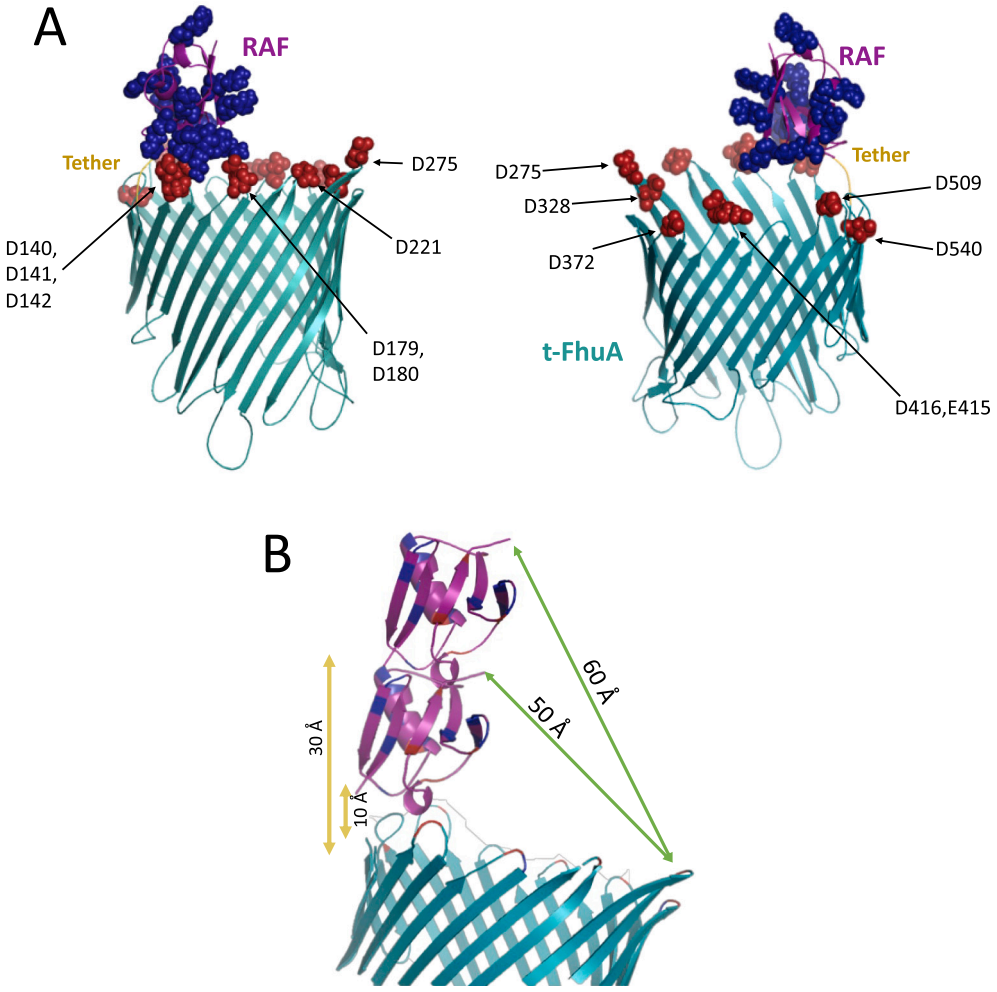

Fig. 6. Cartoon of R6F and CRAF1-RBD attached to the C terminus of t-FhuA via a peptide tether of varying length. (A) CRAF1-RBD was fused to the N terminus of t-FhuA via a Ser/Gly-rich hexapeptide. Positively charged residues and negatively charged residues are shown in blue and red, respectively. Positive residues of the folded CRAF1-RBD domain are exposed to negative residues located on the β turns T1 through T4 and T5 through T10 of t-FhuA on the left-side and right-side panel, respectively. (B) The maximum length of a 3-residue peptide tether in a stretched-out conformation measures ~10 Å, whereas that corresponding length of a 9-residue peptide tether extends to ~30 Å. Therefore, attaching CRAF1-RBD to the C terminus of t-FhuA implies that the distances of the C terminus of the folded CRAF1-RBD domain to the pore opening are ~50 Å and ~60 Å for a short 3-residue peptide tether and a long 9-residue peptide tether, respectively. (For interpretation of the references to colour in this figure legend, the reader is referred to the web version of this article.)

is a key challenging task. For example, it has been previously demonstrated that attaching a biotinylated PEG with two repetitive units, and not eleven repetitive units or forty-five repetitive units, to the noisy loop 6 of OmpG, makes this design sensitive to neutral streptavidin binding [17]. However, all these linker-length designs were sensitive to positively charged avidin binding. This finding suggests that features of an interacting partner plays a pivotal role in altering pore behavior [17,20,47] and the size of the tethering linker for an effective sensor [17].

5. Conclusions

In summary, we show a systematic single-molecule electrophysiology analysis of the insertion substate of modular protein nanopores of varying composition and architecture. These modular nanopores encompass a monomeric β-barrel protein pore fused to an exogenous stably folded protein via a flexible peptide tether of varying length. Furthermore, unstructured polypeptide tails were engineered at the untethered ends of these nanopores. We found that these synthetic nanopores insert predominantly with one out of the three insertion conductance substates: a low-conductance insertion substate, a medium-conductance insertion substate, or a large-conductance insertion substate. Here, we provide compelling experimental evidence that the relative insertion frequency of a given substate depends on key ingredients of the nanopore composition, such as the length of the peptide tether, the nanopore terminus at which the protein fusion was conducted, and the total mass of the tethered protein. With further development, such a new class of modular nanopores can be used in future in the real-time detection of protein-nucleic acid or protein-protein interactions observed in aqueous phase. Finally, these modular protein nanopores could represent the basis for a proteomics setting or might be further extended to create novel tools in biosensor technology.

CRediT authorship contribution statement

M.G.L., S.N.L., and L.M. designed research. M.G.L. performed cloning, as well as protein expression, refolding, and purification. J.H.H. performed cloning. M.G.L. collected, processed, and analyzed single-molecule electrophysiology data. M.G.L. and L.M. wrote the paper.

Declaration of competing interest

The authors declare that they have no known competing financial interests or personal relationships that could have appeared to influence the work reported in this paper.

Acknowledgments

The authors are grateful to Dr. Stephen W. Michnik (University of Montreal) for providing the pQE32 RAF-DHFR plasmid. We also thank people in the Movileanu laboratory for their feedback and constructive comments pertaining to this manuscript. This work was supported by the National Institute of General Medical Sciences of the U.S. National Institutes of Health, grants R01 GM088403 (to L.M.) and R01

GM115762 (to S.N.L.).

Appendix A. Supplementary data

Supplementary data to this article can be found online at https://doi.org/10.1016/j.bbamem.2021.183570.

References

[1] B. Sackmann, E. Neher, Single-Channel Recording, Kluwer Academic/Plenum Publishers, New York, Second Edition ed., 1995.
[2] M. Montal, P. Mueller, Formation of bimolecular membranes from lipid monolayers and a study of their electrical properties, Proc. Natl. Acad. Sci. U. S. A. 69 (1972) 3561–3566.
[3] M.M. Mohammad, L. Movileanu, Excursion of a single polypeptide into a protein pore: simple physics, but complicated biology, Eur. Biophys. J. 37 (2008) 913–925.
[4] R. Bikwemu, A.J. Wolfe, X. Xing, L. Movileanu, Facilitated Translocation of Polypeptides Through a Single Nanopore, J. Phys.: Condens. Matter, 22 (2010) 454117.
[5] D.P. Hoogerheide, P.A. Gurnev, T.K. Rostovtseva, S.M. Bezrukov, Real-time nanopore-based recognition of protein translocation success, Biophys. J. 114 (2018) 772–776.
[6] L.Z. Song, M.R. Hobaugh, C. Shustak, S. Cheley, H. Bayley, J.E. Gouaux, Structure of staphylococcal alpha-hemolysin, a heptameric transmembrane pore, Science 274 (1996) 1859–1866.
[7] K. Willems, D. Ruić, A. Biesemans, N.S. Galenkamp, P. Van Dorpe, G. Maglia, Engineering and modeling the electrophoretic trapping of a single protein inside a nanopore, ACS Nano 13 (2019) 9980–9992.
[8] S. Zernia, N.J. van der Heide, N.S. Galenkamp, G. Gouridis, G. Maglia, Current blockades of proteins inside nanopores for real-time metabolome analysis, ACS Nano 14 (2020) 2296–2307.
[9] G. Huang, K. Willems, M. Bartelds, P. van Dorpe, M. Soskine, G. Maglia, Electro-osmotic vortices promote the capture of folded proteins by PlyAB nanopores, Nano Lett. 20 (2020) 3819–3827.
[10] L. Movileanu, S. Howorka, O. Braha, H. Bayley, Detecting protein analytes that modulate transmembrane movement of a polymer chain within a single protein pore, Nat. Biotechnol. 18 (2000) 1091–1095.
[11] F. van der Goot, S. Matile, Sensing proteins outside of the box, Nat. Biotechnol. 18 (2000) 1037.
[12] D. Rotem, L. Jayasinghe, M. Salichou, H. Bayley, Protein detection by nanopores equipped with aptamers, J. Am. Chem. Soc. 134 (2012) 2781–2787.
[13] L. Harrington, S. Cheley, L.T. Alexander, S. Knapp, H. Bayley, Stochastic detection of Pim protein kinases reveals electrostatically enhanced association of a peptide substrate, Proc. Natl. Acad. Sci. U.S.A, 110 (2013) E4417-E4426.
[14] L. Harrington, L.T. Alexander, S. Knapp, H. Bayley, Single-molecule protein phosphorylation and dephosphorylation by nanopore enzymology, ACS Nano 13 (2018) 633–641.
[15] M. Fahie, C. Chisholm, M. Chen, Resolved single-molecule detection of individual species within a mixture of anti-biotin antibodies using an engineered monomeric nanopore, ACS Nano 9 (2015) 1089–1098.
[16] M.A. Fahie, B. Yang, M. Mullis, M.A. Holden, M. Chen, Selective detection of protein homologues in serum using an OmpG nanopore, Anal. Chem. 87 (2015) 11143–11149.
[17] M.A. Fahie, B. Yang, B. Pham, M. Chen, Tuning the selectivity and sensitivity of an OmpG nanopore sensor by adjusting ligand tether length, ACS Sens. 1 (2016) 614–622.
[18] M. Chen, S. Khalid, M.S. Sansom, H. Bayley, Outer membrane protein G: engineering a quiet pore for biosensing, Proc. Natl. Acad. Sci. U. S. A. 105 (2008) 6272–6277.
[19] M. Chen, Q.H. Li, H. Bayley, Orientation of the monomeric porin OmpG in planar lipid bilayers, Chembiochem. 9 (2008) 3029–3036.
[20] A.K. Thakur, L. Movileanu, Real-time measurement of protein-protein interactions at single-molecule resolution using a biological nanopore, Nat. Biotechnol. 37 (2019) 96–101.
[21] C. Frisch, G. Schreiber, C.M. Johnson, A.R. Fersht, Thermodynamics of the interaction of barnase and barstar: changes in free energy versus changes in enthalpy on mutation, J. Mol. Biol. 267 (1997) 696–706.
[22] G. Schreiber, C. Frisch, A.R. Fersht, The role of Glu73 of barnase in catalysis and the binding of barstar, J. Mol. Biol. 270 (1997) 111–122.
[23] G. Schreiber, A.R. Fersht, Rapid, electrostatically assisted association of proteins, Nat. Struct. Biol. 3 (1996) 427–431.
[24] A.M. Buckle, G. Schreiber, A.R. Fersht, Protein-protein recognition: crystal structural analysis of a barnase-barstar complex at 2.0-a resolution, Biochemistry 33 (1994) 8878–8889.
[25] G. Schreiber, A.R. Fersht, Interaction of barnase with its polypeptide inhibitor barstar studied by protein engineering, Biochemistry 32 (1993) 5145–5150.
[26] C. Frisch, A.R. Fersht, G. Schreiber, Experimental assignment of the structure of the transition state for the association of barnase and barstar, J. Mol. Biol. 308 (2001) 69–77.
[27] G. Schreiber, A.R. Fersht, Energetics of protein-protein interactions: analysis of the barnase-barstar interface by single mutations and double mutant cycles, J. Mol. Biol. 248 (1995) 478–486.
[28] A.K. Thakur, L. Movileanu, Single-molecule protein detection in a biofluid using a quantitative nanopore sensor, ACS Sens. 4 (2019) 2320–2326.
[29] J. Sun, A.K. Thakur, L. Movileanu, Protein ligand-induced amplification in the 1/f noise of a protein-selective nanopore, Langmuir 36 (2020) 15247–15257.
[30] K.P. Locher, B. Rees, R. Koebnik, A. Mitschler, L. Moulinier, J.P. Rosenbusch, D. Moras, Transmembrane signaling across the ligand-gated FhuA receptor: crystal structures of free and ferrichrome-bound states reveal allosteric changes, Cell 95 (1998) 771–778.
[31] M.M. Mohammad, K.R. Howard, L. Movileanu, Redesign of a plugged beta-barrel membrane protein, J. Biol. Chem. 286 (2011) 8000–8013.
[32] D.J. Niedzwiecki, M.M. Mohammad, L. Movileanu, Inspection of the engineered FhuA deltaC/delta4L protein nanopore by polymer exclusion, Biophys. J. 103 (2012) 2115–2124.
[33] M.M. Mohammad, R. Iyer, K.R. Howard, M.P. McPike, P.N. Borer, L. Movileanu, Engineering a rigid protein tunnel for biomolecular detection, J. Am. Chem. Soc. 134 (2012) 9521–9531.
[34] F.X. Campbell-Valois, K. Tarassov, S.W. Michnick, Massive sequence perturbation of the Raf ras binding domain reveals relationships between sequence conservation, secondary structure propensity, hydrophobic core organization and stability, J. Mol. Biol. 362 (2006) 151–171.
[35] A. Wittinghofer, N. Nassar, How Ras-related proteins talk to their effectors, Trends Biochem. Sci. 21 (1996) 488–491.
[36] N. Nassar, G. Horn, C. Herrmann, A. Scherer, F. McCormick, A. Wittinghofer, The 2.2 A crystal structure of the Ras-binding domain of the serine/threonine kinase c-Raf1 in complex with Rap1A and a GTP analogue, Nature 375 (1995) 554–560.
[37] J.N. Pelletier, F.X. Campbell-Valois, S.W. Michnick, Oligomerization domain-directed reassembly of active dihydrofolate reductase from rationally designed fragments, Proc. Natl. Acad. Sci. U. S. A. 95 (1998) 12141–12146.
[38] F.X. Campbell-Valois, K. Tarassov, S.W. Michnick, Massive sequence perturbation of a small protein, Proc. Natl. Acad. Sci. U. S. A. 102 (2005) 14988–14993.
[39] T. Unger, Y. Jacobovitch, A. Dantes, R. Bernheim, Y. Peleg, Applications of the restriction free (RF) cloning procedure for molecular manipulations and protein expression, J. Struct. Biol. 172 (2010) 34–44.
[40] M.G. Larimi, L.A. Mayse, L. Movileanu, Interactions of a polypeptide with a protein nanopore under crowding conditions, ACS Nano 13 (2019) 4469–4477.
[41] S. Couoh-Cardel, Y.C. Hsueh, S. Wilkens, L. Movileanu, Yeast V-ATPase proteolipid ring acts as a large-conductance transmembrane protein pore, Sci. Rep. 6 (2016) 24774.
[42] D. Kudlinzki, A. Schmitt, H. Christian, R. Ficner, Structural analysis of the C-terminal domain of the spliceosomal helicase Prp22, Biol. Chem. 393 (2012) 1131–1140.
[43] J.R. Sydor, M. Engelhard, A. Wittinghofer, R.S. Goody, C. Herrmann, Transient kinetic studies on the interaction of Ras and the Ras-binding domain of c-Raf-1 reveal rapid equilibration of the complex, Biochemistry 37 (1998) 14292–14299.
[44] C.F. Becker, C.L. Hunter, R. Seidel, S.B. Kent, R.S. Goody, M. Engelhard, Total chemical synthesis of a functional interacting protein pair: the protooncogene H-Ras and the Ras-binding domain of its effector c-Raf1, Proc. Natl. Acad. Sci. U. S. A. 100 (2003) 5075–5080.
[45] O.V. Krasilnikov, C.G. Rodrigues, S.M. Bezrukov, Single polymer molecules in a protein nanopore in the limit of a strong polymer-pore attraction, Phys. Rev. Lett. 97 (2006), 018301.
[46] M.M. Mohammad, S. Prakash, A. Matouschek, L. Movileanu, Controlling a single protein in a nanopore through electrostatic traps, J. Am. Chem. Soc. 130 (2008) 4081–4088.
[47] K. Lundquist, J. Bakelar, N. Noinaj, J.C. Gumbart, C-terminal kink formation is required for lateral gating in BamA, Proc. Natl. Acad. Sci. U. S. A. 115 (2018) E7942–e7949.
[48] L. Movileanu, S. Cheley, S. Howorka, O. Braha, H. Bayley, Location of a constriction in the lumen of a transmembrane pore by targeted covalent attachment of polymer molecules, J. Gen. Physiol. 117 (2001) 239–251.
[49] S.K. Fetics, H. Guterres, B.M. Kearney, G. Buhrman, B. Ma, R. Nussinov, C. Mattos, Allosteric effects of the oncogenic RasQ61L mutant on Raf-RBD, Structure 23 (2015) 505–516.